THE ASTROPHYSICAL JOURNAL, 420:326–335, 1994 January 1

"SPHERICAL" DISKS: MOVING TOWARD A UNIFIED SOURCE MODEL FOR L1551

HAROLD M. BUTNER[1]
NASA Ames Research Center, MS 245/6, Moffett Field, CA 94035
ANTONELLA NATTA
Osservatorio Astrofisico di Arcetri, Largo E. Fermi 5, I-50125 Firenze, Italy
AND
NEAL J. EVANS II[2]
Department of Astronomy, The University of Texas at Austin, Austin, TX 78712-1083
Received 1992 August 14; accepted 1993 July 8

ABSTRACT

To predict the effects of a disk on the spectral energy distribution of a deeply embedded protostar, we construct disk models with power-law temperature distributions ($T \propto r^{-q}$). We then use the spherically averaged disk emission as the central source for a spherical envelope, hence the term, "spherical" disk. We then calculate the predicted spectral energy distribution of the disk and envelope, using a spherically symmetric radiative transport code. Applying this procedure to L1551 IRS 5, we find that the predicted far-infrared flux is not very sensitive to the nature of the central source, The best source model is consistent with the far-infrared emission arising from the infalling region in an "inside-out" collapse model, independent of the nature of the central source. Disk models are superior to the star-only model when we try to match millimeter interferometer data. While disks with various q can reproduce the observed 2.7 mm interferometer flux, only an active disk ($q = 0.5$) can produce enough emission in a region small enough to match the observed 2.7 mm visibilities. However, if the disk is backwarmed by the envelope, even purely reprocessing disks can meet this constraint. All types of backwarmed disks are virtually indistinguishable in their millimeter properties. We find that all reasonable envelope models are sufficiently opaque in the mid-infrared to attenuate any disk model to a level well below the observations, unless the ratio of the mid-infrared to far-infrared dust opacities is similar to that of the dust opacities advocated by Mathis, Mezger, & Panagia (1983).

Subject headings: accretion, accretion disks — ISM: individual (L1551 IRS 5) — stars: pre–main-sequence

1. INTRODUCTION

Current theories for the formation of low-mass stars (e.g., Shu, Adams, & Lizano 1987) envision a sequence of events, including quasi-static formation of a cloud core, with collapse beginning at the center of the core, leading to the growth of an infall zone, from which material falls onto the central region. If some initial rotation exists, centrifugal forces can prevent most of the matter from falling directly onto the new star; instead it falls first onto a thin disk (Terebey, Shu, & Cassen 1984). Material in the disk gradually moves through the disk and then accretes onto the central star. The infall phase ends when either the surrounding envelope is exhausted or the newborn star, through the action of winds, disrupts the prenatal envelope and stops the infalling material. Such models have four basic regions: a quiescent envelope, where density declines with radius as in an isothermal sphere ($n \propto r^{-2}$), an infall zone ($n \propto r^{-1.5}$), a disk, and a central star.

As a test of the theory, Adams, Lada, & Shu (1987) used a radiative transport code to model a number of nearby young stellar objects. They found that the Terebey et al. model could produce spectral energy distributions consistent with the observations, except at the very shortest infrared wavelengths, where the observations had more emission than the models. The discrepancy is probably caused by scattering (Moneti et al. 1988), which was not included in the models. Butner et al. (1991) modeled the spatial distribution of the far-infrared emission of L1551 IRS 5 by calculating the radiative transport and dust temperatures using only spherical envelope models. The best agreement with the far-infrared observations was found for a model which had $n(r) \propto r^{-1.5}$, the exponent being in excellent agreement with the predictions of Adams et al. (1987), and just what is expected if the envelope is still undergoing infall. The model also matched most of the observed characteristics of the spectral energy distribution if the dust grain opacities favored by Mathis, Mezger, & Panagia (1983, hereafter MMP) were adopted. Ladd et al. (1991) have extended the Adams et al. (1987) models to a number of new low-mass objects and found that models based on the ideas of Terebey et al. (1984) could also be constructed for these sources.

These successes have been one factor in the widespread acceptance of the idea that disks surround young stars. In particular, Adams et al. (1987) argued that a disk was necessary to produce enough emission to match observations at mid-infrared ($5 < \lambda < 20$ μm) wavelengths, where scattering should play a smaller role. Subsequently, many workers have assumed that all emission from young objects, in excess of that expected from the star, arises in a disk. However, Butner et al. (1991) found that uncertainties in our current knowledge of dust opacities are sufficient to call into question the need for a disk in

[1] Postal address: Carnegie Institute of Washington, Department of Terrestrial Magnetism, 5241 Broad Branch Road, NW Washington, DC 20015-1305.
[2] E-mail:nje@astro.as.utexas.edu

the case of L1551 IRS 5, and by extension, in other deeply embedded objects, *based on their mid-infrared emission.* In particular, if MMP dust opacities were adopted, the star+envelope models provided an excellent match to the mid-infrared emission, challenging the argument of Adams et al. (1987) that only a disk (or other compact source) could explain the mid-infrared emission. In addition, Butner et al. (1991) pointed out that the far-infrared emission in L1551 IRS 5 was extended, ruling out its origin in a disk. A similar conclusion was reached for the far-infrared emission from a number of Herbig Ae/Be stars (Natta et al. 1992, 1993). These results suggest that careful analysis of these sources, including the emission from an envelope, are needed before definitive conclusions about disks can be made from the spectral energy distribution (see also Hillenbrand et al. 1992; Kenyon & Hartmann 1991; Hartmann, Kenyon, & Calvet 1993). The need to understand the relative contribution that disks and envelopes make to the spectral energy distribution motivates this paper, which will attempt to include both disk and envelope in models of the infrared emission from deeply embedded young objects.

We will first construct three types of disk models, all with power law temperature distributions. We will then use the radiation field from the disk models averaged over all angles as the luminosity source for a spherical envelope. We focus our attention on three questions; what observed quantities can be useful diagnostics for the presence of a disk; what effect does the central source have on derived envelope properties; and what effect can an envelope have on the inferred properties of the disk. We will apply these models to L1551 IRS 5, a source for which abundant data, as well as a testable model, exist.

The one striking failure for the original spherical envelope model of Butner et al. (1991) was its inability to match millimeter interferometer measurements (Keene & Masson 1990), which indicate that about half the flux density at 2.7 mm comes from a compact source. Theoretically, the most attractive candidate for the compact source is a disk, but other compact structures are possible in principle. If a compact structure is present, it might also contribute enough far-infrared emission to change the conclusions reached by Butner et al. (1991) that the density gradient in the envelope is $n(r) \propto r^{-1.5}$. Hence, we examine whether the presence of a disk could alter the density gradient derived by Butner et al. (1991) from the 100 μm data.

In addition, L1551 IRS 5 is an object where the optical depth of the surrounding envelope is high and the inner walls of the envelope are warm compared to the outer regions of the disk. Under such conditions, Keene & Masson (1990) suggested that a disk inside an envelope could not become colder than the temperature at the inner edge of the envelope. We will consider models in which this "backwarming" effect is included and determine how significantly the disk properties change.

2. MODELS FOR THE COMPACT SOURCE

2.1. *Disk Models*

In this section, we construct different disk models which are all constrained to match the 2.7 mm flux seen within the interferometer beam (2.″6 or 415 AU) of Keene & Masson (1990). The disk can be considered independently of any envelope when matching the interferometric observations since all acceptable envelope models predict negligible flux inside the interferometer beam (Butner et al. 1991).

Since no self-consistent radiative transport models are available for disks and since the question of the true source of the disk luminosity is unresolved, we follow Beckwith et al. (1990) in adopting a heuristic disk model. We use their prescription for specifying the properties of the disk. Each disk is characterized by its inner (r_0) and outer (R_d) radii, and by its inclination with respect to the line of sight (θ). The dependence of surface density on radius is assumed to be a power law:

$$\Sigma(r) = \Sigma_0 (r/r_0)^{-p} . \quad (1)$$

We follow Beckwith et al. (1990) in adopting $p = 1.5$. For a discussion of reasonable values for this parameter, see Adams, Lada, & Shu (1988). We also adopt the dust opacities of the disk material used by Beckwith et al. (1990):

$$\kappa_\nu = \kappa_{12} (\nu/10^{12} \text{ Hz})^\beta , \quad (2)$$

with the dust mass extinction coefficient at 10^{12}Hz defined to be $\kappa_{12} = 0.1$ cm^2 g^{-1} and $\beta = 1$. In fact, most of our models will turn out to be optically thick at all wavelengths of interest, making both the opacity law and the disk surface density gradient irrelevant in computing the emission from the disk. However, the opacity (and the assumed surface density gradient) will affect the mass derived for the disk. Since Σ_0 is constrained by the need to keep the disk opaque enough at its outer edge to produce the 2.7 mm emission, the model Σ_0, and hence M_d, the disk mass, depend on the assumed opacity. If the optical depth to the observer at frequency ν is constrained to be τ_ν at the edge of the disk (R_d), the required mass is

$$M_d = 2\pi \frac{\tau_\nu \cos\theta}{\kappa_{12}} \left(\frac{\nu}{10^{12}}\right)^{-\beta} R_d^p \frac{(R_d^{2-p} - r_0^{2-p})}{(2-p)} , \quad (3)$$

for $p \neq 2$. For $p < 2$ and $R_d \gg r_0$, which apply to all our models, it is adequate to approximate the dependences as

$$M_d \propto \frac{R_d^2}{(2-p)} (\kappa_{12})^{-1} , \quad (4)$$

illustrating the fact that variations in the assumed p from 1.5 to zero will change the derived M_d by only a factor of 4, comarable to the uncertainties in κ_{12}.

The disk has at its center a star with luminosity L_*; by assuming the star to be a blackbody at temperature T_*, the stellar radius r_* is determined. We calculate the temperature distribution in the disk starting from equation (12) of Adams et al. (1988), which includes the effects of reprocessed stellar radiation as well as an intrinsic disk luminosity which can produce an arbitrary power law in the temperature distribution. In our formulation below, we have replaced their variable ϖ by r. We adopt their assumption of an infinitely thin disk and thus we neglect the possible effects of increasing vertical height in the disk with radius. For a discussion of the effects of flared disks, see Kenyon & Hartmann (1987, 1991) and Calvet et al. (1992). We also ignore any vertical temperature distribution; see Calvet et al. (1992) for analysis of this problem in flared disks. Given these assumptions and approximations, the resulting T is calculated in terms of $u = r_*/r$ by

$$T(u) = \left\{ \frac{L_{\rm int} u^{4q}}{4\pi\sigma r_*^2 \Upsilon} + \frac{T_*^4}{\pi} [\arcsin u - u(1-u^2)^{0.5}] \right\}^{1/4} , \quad (5)$$

where $L_{\rm int}$ is the intrinsic disk luminosity, which is assumed to produce a temperature distribution, $T = T_0 (r/r_0)^{-q}$, if reprocessing is neglected. The quantity T_0 is the temperature at r_0,

the inner radius of the disk. The function Υ is given by

$$\Upsilon = \begin{cases} \ln\left(\frac{R_d}{r_0}\right) & q = \frac{1}{2} \\ \frac{1-(r_0/R_d)^{4q-2}}{4q-2} & q \neq \frac{1}{2} \end{cases} . \quad (6)$$

For all models, we assume that $\theta = 45°$ (Stocke et al. 1988) and that the distance to the source is 160 pc (Snell 1981). We also assume a stellar temperature of $T_* = 5500$ K (Stocke et al. 1988) and a total source (star+disk) luminosity of 28 $L_\odot$. Depending on the source model, the stellar radius (r_*) can vary between 1 and 6 $R_\odot$. The assumed T_* is the hottest component deduced from the visual and near-infrared photometry. However, as Stocke et al. (1988) point out, the true stellar temperature is not well defined. The disk has a range of temperatures, and can even be hotter than the stellar surface due to luminosity generated within the disk by viscous accretion or other processes. In addition, if accretion onto the stellar surface is occurring, there is a boundary layer present. Fortunately, our models are insensitive to the stellar temperature assumed. As we discuss in § 3, the radiation field is rapidly reprocessed by the optically thick envelope ($A_V \geq 100$). When we vary the central source temperature between 3000 and 8000 K, we find that the predicted spectral energy distributions are virtually identical.

We also assume that the disk begins at the stellar surface ($r_0 = r_*$). For some models, this assumption results in temperatures which are larger than those at which dust grains should vaporize. However, the disk is likely to continue into r_* in gaseous form and the gas may still be opaque at the high surface densities of our models (e.g., Hartmann et al. 1993). At any rate, this assumption does not affect the emission at long wavelengths which is of primary interest to us, as the millimeter emission arises from a much cooler portion of the disk; and the short wavelength emission from this inner, hot region will be completely attenuated by the surrounding envelope.

To calculate the flux expected from the disk, we first divide the disk into a large number of radial sections. For each section, we calculate the temperature [$T(u)$] using equation (5). The disk optical depth at u for a given wavelength is calculated, and we evaluate

$$I_\nu(u) = B_\nu[T(u)](1 - e^{-\tau_\nu}) , \quad (7)$$

for each radius and each wavelength. The flux is then calculated and summed over all disk radii. We also add the stellar contribution to the flux. We calculate both the average radiation field, equivalent to a viewing angle of 60°, and the radiation field seen at 45°. We need the average for our envelope models (§ 3), and the 45° model to compare with observations.

2.2. *Three Flavors of Disk*

First, we consider passive, reprocessing disks, with $L_* = 28\ L_\odot$, $r_* = 6\ R_\odot$; these produce a temperature which decreases as $r^{-0.75}$ at large radii. The free parameters are then the fiducial surface density (Σ_0), or equivalently the mass of the disk M_d, and the outer radius R_d. We first define the smallest R_d which matches the observed $S_\nu(2.7\ \text{mm}) = 0.13 \pm 0.03$ Jy by setting M_d large enough to make the disk opaque at 2.7 mm all the way out to R_d. The resulting $R_d = 167$ AU (1".1); if we only require that the model match the observations within 1 σ, R_d can shrink to 130 AU. We also tried to minimize M_d by decreasing Σ_0 while keeping $R_d = 167$ AU; the resulting minimum mass is 1.6 $M_\odot$. These values (summarized in Table 1) thus represent fairly conservative limits, except that, as noted above, M_d also depends on the assumed dust opacity and the power law in the surface density (p). The minimum radius is considerably larger than the value ($\sim$40 AU) favored both by the Adams et al. (1987) model and by Keene & Masson (1990).

Next, we consider disks with intrinsic luminosity, which we constrain by requiring that the total (star+disk) luminosity ($L_{\rm tot} = L_* + L_{\rm int}$) be the observed value. First, we consider a standard, viscous accretion disk model (henceforth referred to as the viscous disk). Such a model will still have $q = 0.75$, but the disk temperature may be higher than the reprocessing disk. To take an extreme case, we can put essentially all the observed luminosity into the disk ($L_{\rm int} = 27\ L_\odot$ and $L_* = 1\ L_\odot$). The central stellar radius is then only 1 $R_\odot$. This model still requires a large disk radius ($R_d \geq 140$ AU) and a large mass ($M \geq 0.9\ M_\odot$). Varying the relative intrinsic luminosities of the star and the disk can modify R_d. For these models, the star's radius shrinks as stellar luminosity decreases since the stellar temperature is fixed. Hence, for our models there is a trade-off in the outer disk temperatures between the heating effects of high disk luminosities and the scaling of the temperature at a given physical radius downwards due to a smaller stellar radius ($r_0 = r_*$). For lower T_0, a larger R_d is required if we are to match the observed emission at 2.7 *mm*, which comes from the outer part of the disk. For the $q = 0.75$ case, the smallest R_d (135 AU) that reproduces the 2.7 mm emission occurs when about half the total system luminosity is assigned to the star ($L_* = 14\ L_\odot$, $r_* = 4\ R_\odot$). As in the case of the purely reprocessing disk, we then minimize R_d by requiring the models to match the interferometer observations within 1 σ (0.10 Jy at 2.7 mm) for an optically thick disk. We also minimize the mass (M_d) while fixing R_d at 135 AU (the value required to match the interferometer fluxes) and then we decrease the surface density until we dropped the predicted flux by 1 σ (i.e., to 0.10 Jy). The results, given in Table 1, show that the required size and mass of the disk are still quite large.

Finally, we consider disks with the flatter temperature distribution ($q = 0.5$) favored by Adams, Lada, & Shu (1988). We will refer to these disks as "active." While this temperature distribution is somewhat ad hoc, it has been widely invoked to

TABLE 1

DISK PARAMETERS

Disk Type	q	$L_{\rm int}$ ($L_\odot$)	R_d (AU)	min R_d[a] (AU)	min M_d[b] ($M_\odot$)	$T(R_d)$ (K)
Reprocessing	0.75	0	167	>130	>1.6	5.4
Viscous	0.75	14	135	>106	>1.1	7.6
Active	0.50	14	45	>37	>0.14	69
Reprocessing[c]	0.75	0	59	>47	>0.28	95
Viscous[c]	0.75	14	48	>40	>0.19	103
Active[c]	0.50	14	43	>36	>0.15	108

[a] Minimum R_d determined by decreasing R_d of an optically thick disk until the model flux density was 1 σ below the observations.

[b] Minimum M_d determined by keeping R_d fixed to the size required for an optically thick disk to match the 2.7 mm interferometer observations, and then decreasing the surface density (Σ_0) until the model flux density was 1 σ below the observations.

[c] These disks include backwarming from the envelope, as discussed in the text.

explain spectral energy distributions of less embedded objects, such as T Tauri stars (Beckwith et al. 1990). Suggestions for how this distribution might arise include both eccentric gravitational instabilities (Adams, Ruden, & Shu 1989) and strongly flared disks (Kenyon & Hartman 1987, 1991). In the case of the flared disk, the mechanism is not internal energy but enhanced reprocessing at large radii, due to the flare; consequently, $q = 0.5$ is achieved only at fairly large radii. The flared disk model could only account for disk models where the inferred disk luminosity is a fraction of the total source luminosity. Since we are not concerned here with the exact physical mechanism responsible, but only with the final spectrum, we consider disks where $q = 0.5$ at all radii. Again assigning nearly all the luminosity to the disk ($L_{\rm int} = 27\ L_\odot$), we find a minimum $R_d = 35$ AU, to match the observations to within 1 σ. In this case, this limit produces the smallest R_d, but the results are not very sensitive to the fraction of the total luminosity assigned to the disk. For $L_{\rm int} = 7\ L_\odot$, the minimum $R_d = 42$ AU. For $L_{\rm int} = L_* = 14\ L_\odot$, $r_* = 4\ R_\odot$, and $R_d = 43$ AU; the minimum $R_d = 37$ AU and the minimum $M_d = 0.14\ M_\odot$ (see Table 1). Clearly, the flatter temperature law allows a much more modest mass in the optically thick disk, as well as allowing an outer radius which is very consistent both with the model of Adams et al. (1987) and with the considerations of Keene & Masson (1990).

As input into the radiative transport code for the envelope, we use the three disk models in which we actually match the 2.7 mm flux density precisely, rather than the models with the minimum R_d. The differences in the emission spectra are never substantial, although the masses are of course larger than they would be in the $R_{\rm min}$ or $M_{\rm min}$ cases. We show in Figure 1*a* the spectral energy distributions produced by a star, combined with the three disk models, as well as that produced by the star alone. We also show the peak flux densities in the interferometer beams at 1.3 mm (Sargent 1991), 1.36 mm (Woody et al. 1989), and 2.7 mm (Keene & Masson 1990). By design, all the models with disks match the interferometer flux at 2.7 mm, but only the active disk comes close to reproducing the interferometer flux at 1.3 mm. Since we plot S_ν, the active disk does not produce a "flat" profile, but rather a profile which rises with increasing λ at mid-infrared wavelengths. Beyond about 100 μm, the emission decreases because the disk cuts off at $R_d = 45$ AU, leading to a minimum T and hence a decrease in S_ν (see Adams et al. 1988). In contrast, the passive disk and the viscous accretion disk have spectral energy distributions which drop slowly with increasing λ and decrease sharply only at λ greater than about 1000 μm, because their larger R_d allow lower T_d. The dust temperature at the edge of the disk, $T_d(R_d)$, is given in Table 1. Because of these differences, to produce the required emission at 2.7 mm, the active ($q = 0.5$) disk must also generate much more emission at 100 μm. If the disk is bright enough, it might alter the envelope properties that we derived from the observed far-infrared emission (Butner et al. 1991).

2.3. *Spherical Source Models*

Other physical structures could explain the millimeter emission detected by Keene & Masson (1990). Since the source is not resolved, there is no observational constraint that it must be a disk, although a disk is certainly the most plausible theoretically. It is instructive to consider a large cool blackbody as a limiting case of a more spherical compact source. This could represent the inner regions of the infall zone in a perfectly spherically symmetric collapse (Shu 1977). Such a source would be consistent with Terebey et al. (1984) picture if the original cloud rotation was very small.

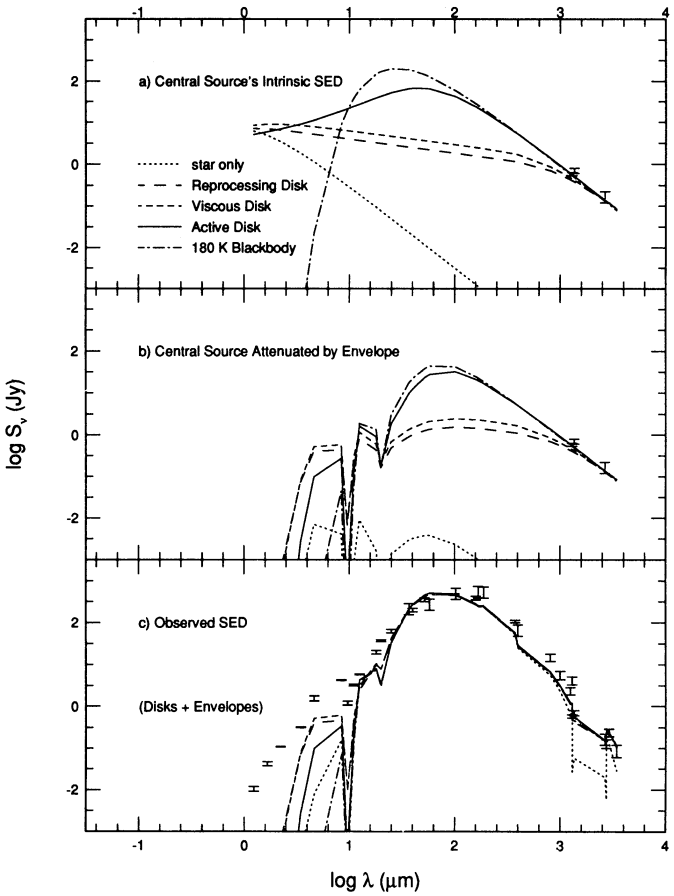

FIG. 1.—In this three panel figure, the top panel (*a*) shows the intrinsic spectral energy distributions of the different central sources ($L^{\rm tot} = 28\ L_\odot$): the dotted line is the star-only model; the long dashed line is the reprocessing disk ($L_{\rm int} = 0$) plus star; the short dashed line is the viscous disk ($L_{\rm int} = 14\ L_\odot$ and $q = 0.75$); and the solid line is the active disk ($L_{\rm int} = 14\ L_\odot$ and $q = 0.5$). The properties of the disks are given in Table 1. The dash-dotted line is the predicted spectral energy distribution for an 180 K blackbody with 28 $L_\odot$. The three data points are interferometric observations at 1.3 mm (0.58 Jy, 1".6 beam, Sargent 1991), 1.36 mm (0.70 Jy, 3".3 beam, Woody et al. 1989), and 2.7 mm (0.13, Jy, 2".6 beam, Keene & Masson 1990). The middle panel (*b*) shows the predicted spectral energy distributions of these disks (lines coded in the same way) attenuated by the envelopes with the properties described in Table 2. The bottom panel (*c*) shows the full spectral energy distributions of the central source plus envelope, for envelopes with $n(r) \propto r^{-\alpha}$ and inner radii ($R_{\rm inner}$) given by the outer radii of the disks (see Table 2). The star+envelope model parameters are taken from the best ALS model in Butner et al. (1991), model G3. For the models with disks, we have retained $\alpha = 1.5$, but we have adjusted τ_{100} to match the flux density at 100 μm and the dust opacity law at long wavelengths so that the model predictions for fluxes in big beams match the observations at $\lambda > 1$ mm. The bottom panel also shows the observed spectral energy distribution with uncertainties, taken from Butner et al. (1991).

It is trivial to show that the flux density from a blackbody which is constrained to produce the observed luminosity depends only on the source luminosity and temperature. Because the maximum source radius is limited to

$$r^2 = \frac{L}{4\pi\sigma T^4}\,, \tag{8}$$

and the flux density S_ν is $\propto r^2 T$ in the Rayleigh-Jeans limit (valid at 2.7 mm for relevant temperatures), we have $S_\nu \propto T^{-3}$.

The observed 2.7 mm flux $S_\nu = 0.13$ Jy and the total source luminosity of 28 $L_\odot$ then permits a maximum central blackbody $T = 180$ K, with a corresponding minimum radius of 26 AU.

3. COMPACT SOURCES INSIDE ENVELOPES

3.1. *Basic Method: The "Spherical" Disk*

The task of this section is to combine the emission of a disk with that of the spherical envelope. A disk poses an immediate problem for radiative transfer modeling. No fully self-consistent radiative transport models are available for disks, let alone disks inside spherical envelopes. The simplest expedient is to add the emission from a disk to that of the spherical envelope. For example, Keene & Masson (1990) added the emission from a disk model to that from an envelope whose temperature profile was assumed to be that of an optically thin envelope, $T(r) \propto r^{-0.5}$.

We can improve their model by calculating the radiative transfer, and thus the temperature, through the envelope without the optically thin assumption. To include the radiation from the disk, we take the central source to be the radiation field of the star and the disk, averaged over inclination angle. We refer to this spherically averaged radiation field as a "spherical disk" model. The error introduced by this approximation is not large, as long as the disk region which emits most of the radiation which heats the envelope is small compared to the inner radius of the envelope. In this case, any given point in the envelope sees the emission of every point on the disk from the same viewing angle. However, points in a shell of the envelope, at the same distance from the center, will see different amounts of disk emission and, therefore, reach different temperatures. Nonetheless, we found that the net effect of the variation in temperature is small, assuming that most of the heating is done by photons in the Wien limit ($h\nu/kT > 1$). We found that the average flux emitted by the shell, obtained by integrating the emission over the range of temperatures in the shell, is within 30% of the value computed using the spherical disk approximation. As with previous models by Adams et al. (1987) and Butner et al. (1991), we do not expect to fit the near-infrared observations because we do not include the role of light scattered out along the outflow axes.

The radiative transport in the model is computed with a modified version of the code of Egan, Leung, & Spagna (1988), as described by Butner et al. (1991). The dust is assumed to have the opacities given by Adams et al. (1987). The density in the envelope is assumed to follow a power law [$n(r) \propto r^{-\alpha}$], with $\alpha = 1.5$. The inner edge of the envelope in the code ($R_{\rm inner}$) is adjusted to equal the outer radius of the disk (R_d). The temperature at the inner edge of the envelope ($T_{\rm inner}$) is calculated by the radiative transfer code. We adopt a standard outer radius of 100″ (0.08 pc) for the envelope (Butner et al. 1991). The total optical depth of the dust at 100 μm from the outer edge of the envelope to the inner edge (τ_{100}) is adjusted until the model emission at 100 μm matches the observed flux density. For the case of a star only ($L_* = 28\ L_\odot$, $T_* = 5500$ K, and $r_* = 6\ R_\odot$), we adopt the best envelope model parameters from Butner et al. (1991), their model G3. The envelope parameters are summarized in Table 2.

Before we can compare the model spectral energy distribution of the envelope with the observations, we have to add the emission from the central source, as attenuated by the envelope. When adding the emission from a disk, we calculate it for a viewing angle of 45°, the nominal value for L1551 IRS 5.

TABLE 2

ENVELOPE PARAMETERS

Central Source	α	$R_{\rm inner}$ (AU)	$T_{\rm inner}$ (K)	$T_{\rm eff}$ (K)	τ_{100} (ALS)	τ_{100} (DL)	τ_{100}[a] (MMP)
Stellar (G3)	1.5	42	240	...	0.30	0.30	0.39
Reprocessing	1.5	167	130	...	0.15	0.15	0.25
Viscous	1.5	135	135	...	0.16	0.16	0.26
Active	1.5	45	200	...	0.28	0.28	0.36
Blackbody	1.5	26	175	...	0.35	0.35	0.46
Reprocessing[b]	1.5	59	197	94	0.23	0.23	0.30
Viscous[b]	1.5	48	205	101	0.26	0.26	0.34
Active[b]	1.5	43	202	104	0.28	0.28	0.36

[a] These models have $\alpha = 1.2$, rather than 1.5.

[b] These models include backwarming from the envelope in calculating the spectrum of the disk.

3.2. *Results*

The envelope has two effects on the spectral energy distributions: first, the emission from the disk and star is attenuated at $\lambda < 100$ μm, as shown in Figure 1*b*; second, the envelope adds its own emission, which dominates that of the attenuated disk and star for $20 < \lambda < 500$ μm. The spectral energy distributions in Figure 1*c* include the emission from disk, star, and envelope. For comparison, we also show a model with only the star and envelope from Butner et al. (1991). Figure 1*c* also includes the observed emission at various wavelengths. In general the mid-infrared emission was observed with small beams (5″–10″), while the far-infrared emission (50–450 μm) was observed with beam sizes larger than 20″. The millimeter data points were taken primarily with large beams ($\geq$20″), except for three interferometer points at 1.3 mm (0.58 Jy, 1.″6 beam, Sargent 1991), 1.36 mm (0.70 Jy, 3.″3 beam, Woody et al. 1989) and 2.7 mm (0.13 Jy, 2.″7 beam, Keene & Masson 1990). Though only one-tenth the beam size of the other millimeter observations, the interferometer measurements contain almost half the total big beam flux at 2.7 mm. The reader is referred to Table 2 in Butner et al. (1991) for more details about the observations used in the spectral energy distribution. Compared to the disk models, the model with only a star as the central source fails badly at long wavelengths, especially in the small beams (the dips at millimeter wavelengths in the spectral energy distribution for the star-only model correspond to the interferometer points at 1.3, 1.36, and 2.7 mm).

Though less obvious, the original Butner et al. (1991) star-only model also falls below the large-beam observations at millimeter wavelengths. As noted by Butner et al. (1991), this problem can be solved by appropriate modifications to the opacity law at long wavelengths. The dependence of κ_ν on ν at long wavelengths is assumed by Adams et al. (1987) to be ν^2; a smaller exponent is needed to match the 2.7 mm observations in big beams, where about half of the emission comes from the envelope. Pollack et al. (1994) have proposed a model for dust opacities, in which troilite (FeS) is a major opacity source at millimeter wavelengths, producing a ν^1 dependence around 1 mm. We adopt a $\kappa_\nu \propto \nu^1$ dust opacity law for $\lambda > 700$ μm. Using this modified dust opacity for the models with disks and stars, it is possible to match both the large and small beam flux densities at millimeter wavelengths, as shown in Figure 1*c*.

For wavelengths between about 12 and 500 μm, the spectral energy distributions of the models with disks are essentially indistinguishable from those with only the star, since the envelope dominates. This fact can be seen by comparing Figure 1*c* with Figure 1*b*, which shows the emission from the disk plus star attenuated by the envelope, but without the envelope's contribution to the total emission. While the models with disks do produce more emission in the mid-infrared than models without disks, none of these models produce enough emission at $\lambda < 30$ μm to overcome the heavy attenuation by the envelope. Thus, the mid-infrared flux deficit of the envelope models, originally used by Adams, Lada, & Shu (1987) to argue for a disk for L1551 IRS 5, *cannot* be simply remedied by putting a disk inside a spherical envelope.

In the case of larger disk models (the reprocessing and viscous disks), the inner edge of the envelope is moved out to accommodate the larger disk size, because we have adopted $R_{\rm inner} = R_d$. The available data do not tightly constrain $R_{\rm inner}$. To avoid producing too much 100 μm emission from the envelopes with large $R_{\rm inner}$, the total optical depth of the envelope had to be reduced ($\tau_{100} = 0.15$). The lower τ_{100} means that more of the disk radiation gets out, without being reprocessed by the surrounding envelope, as reflected in the stronger emission from the reprocessing and viscous disks in Figures 1*b* and 1*c* at $\lambda < 12$ μm. As can be seen in Figure 1*a*, the mid-infrared emission of the reprocessing and viscous disks is actually weaker than the emission of the active disk. *It is the envelope optical depth that controls the amount of disk flux that can escape from the center of the envelope.* Thus, the effects on the spectral energy distribution of adding disks and envelopes together are fairly complex and involve the interactions between the disk and envelope, subject to constraints introduced to match the observations at specific wavelengths. Simply adding disk emission to envelope emission, without considering the interactions, could lead to erroneous conclusions.

The model with a blackbody for the central source produces more emission around 20 μm, but still not enough to match the observations, and it fails badly at $\lambda < 8$ μm, where its intrinsic emission is too weak. The enhancement in the 20 μm emission is less than one might expect, partly because the optical depth of the envelope had to be increased to $\tau_{100} = 0.35$ to match the observed emission at 100 μm, as a result of the smaller $R_{\rm inner}$ for the blackbody. Despite this smaller $R_{\rm inner}$, the temperature at the inner edge of the envelope ($T_{\rm inner}$) is lower than that of the stellar model because the spectrum of the cool blackbody peaks at much longer wavelengths, so that the heating of the inner edge of the envelope by the central source is less effective.

3.3. *Comparisons with Observations of Spatial Extent*

To distinguish between the different disk models, we consider the spatial distribution of the emission. We use as observational constraints the scans of the source at 50 and 100 μm (Butner et al. 1991), the single dish map at 1.3 mm (Keene & Masson 1990), and the interferometer data at 2.7 mm (Keene & Masson 1990). Comparison of the various models with the far-infrared data do not clearly distinguish between the possibilities; as long as the inner radius of the envelope is less than about 3″ (480 AU), the fit to the scans is acceptable. In addition, the fits to the Keene and Masson 1.3 mm data are also acceptable for all of the models with disks; as shown by Butner et al. (1991), models without a disk produced an intensity distribution at 1.3 mm which was broader than the data of Keene & Masson. However, the 1.3 mm big beam observations cannot be used to distinguish between the different types of disks.

The interferometer data at 2.7 mm can probe smaller scales. A source small enough to be resolved on all baselines of the interferometer would produce a flat visibility function, while a resolved source would produce a decreasing visibility function. We show in Figure 2 the observed visibilities versus projected baseline, taken from Keene & Masson (1990). There is clearly both a resolved source and an unresolved (or barely resolved) source present. We have calculated the predicted visibilities for each of our standard disk and envelope models by convolving the intensity distribution with the primary beam of Keene & Masson (1990) which is assumed to be a Gaussian beam with a half-power full-width of 64″. We then transform our model intensities into visibilities. The disk model visibilities are shown in Figure 2, as is an envelope-only model. As expected from the failure of the envelope-only model to match the interferometer flux, it fails completely to match the visibilities at large baselines, in agreement with the conclusions of Keen & Masson (1990). While all the disk models produce the peak flux seen by the interferometer, the bigger disks produce a decrease in visibilities at large baselines which is inconsistent with the data. Only the active disk and the blackbody are small enough

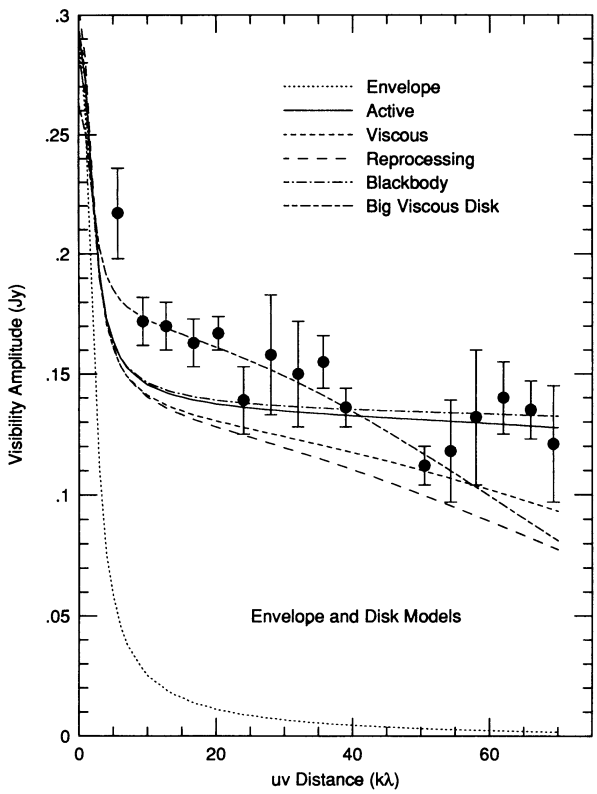

FIG. 2.—Visibility amplitudes at 2.7 mm, taken from Figure 3 of Keene & Masson (1990), are plotted vs. projected baseline. The predicted visibility amplitudes from models with various central sources and envelopes are shown as lines, with the line coding shown in the upper part of the figure. The envelope model contains only a star for a central source, but its flux has been scaled up to match the observed big beam flux. The models with active, viscous, and reprocessing disks are those whose spectral energy distributions are shown in Fig. 1*c*. The blackbody has the properties in Table 1. The big viscous disk is a model with $R_d = 199$ AU; it produces a flux density in the interferometer beam of 0.20 Jy.

to match the observed visibilities at the largest spacings. Thus, the visibility data at large spacings are able to constrain source parameters on scales smaller than the beam.

To test the robustness of the conclusions based on comparisons between our model and the visibility data, we also show a viscous disk model with a larger radius (199 AU) and thus a larger total flux density at 2.7 mm (0.20 Jy). This model (labeled the big, viscous disk in Fig. 2) agrees with the observed visibilities between 10 and 50 kλ, but still falls short for larger baselines. While we have not explored parameter space exhaustively, it does seem that only quite small disks can be consistent with the interferometer data at large baselines.

All of the models match the big beam (60″) flux of 0.29 Jy, but they all fall below the observed visibilities at 7–25 kλ. Interestingly, the model with the big viscous disk does better in this range, but still falls short of the point at 7 kλ. This result indicates that the distributions of emission from the envelopes of the models do not match the observations. Examination of Figure 3 of Keene & Masson (1990) shows better agreement with their simple model of a spherical Gaussian core and a power law envelope. We will reconsider this situation in § 5; for now we focus on the visibilities at large spacings which constrain the size of the compact source.

4. THE EFFECTS OF BACKWARMING

We now consider the idea forwarded by Keene & Masson (1990) that the temperature of a disk inside an opaque envelope cannot fall below the temperature of the inner radius of that envelope. Effectively, the envelope provides a cavity which prevents the escape of disk radiation into free space, thereby "backwarming" the disk. The amount of backwarming depends on the opacity of the envelope and the fraction of the solid angle that the envelope subtends. Since there is an outflow, part of the envelope has been removed, and rotation will cause some flattening of the envelope even before outflow. Thus, the picture of Keene and Masson is one extreme in a continuum of possibilities, the other extreme being represented by the usual disk models which ignore this effect completely. The models of viscous and reprocessing disks without backwarming can produce very low T_d at the outer edge of the disk (see Table 1), so the differences may be substantial. To explore the effects of backwarming, we have computed models which attempt to take it into account.

By approximating the envelope as a blackbody located 40 AU from the star, Keene and Masson derived a temperature of 150 K for the inner edge of the envelope. They then proposed a disk whose temperature fell as $r^{-0.75}$ until it reached 150 K, after which the temperature remained at 150 K. Even if the envelope completely surrounds the disk, this calculation will overestimate the effect unless the envelope is completely opaque at all wavelengths. Using our envelope models, we can assess more accurately the importance of backwarming. For each model, we compute the total emission provided to the disk by the envelope,

$$I_\nu = \int_0^{\tau_\nu(\mathrm{env})} B_\nu[T(r)] e^{-\tau_\nu} d\tau'_\nu , \qquad (9)$$

where τ_ν(env) is the total optical depth of the material in the envelope and τ_ν is the optical depth from the inner edge of the envelope to point of integration (r), where the Planck function $\{B_\nu[T(r)]\}$ is being evaluated, using the envelope temperature calculated by the radiative transfer code. The final envelope emission inside the cavity then is characterized by a blackbody at an effective temperature T_{eff}. This effective temperature is then added to the equation for the disk temperature:

$$T(u) = \left\{ \frac{L_{\mathrm{int}} u^{4q}}{4\pi\sigma r_*^2 \Upsilon} + \frac{T_*^4}{\pi} [\arcsin u - u(1-u^2)^{0.5} + T_{\mathrm{eff}}^4] \right\}^{1/4} . \qquad (10)$$

The net effect of adding this term is to set a lower limit to the disk temperature, just as assumed by Keene & Masson, but this minimum temperature was somewhat lower than they assumed. Since most of the emission at 2.7 mm arises from the parts of the disk where the temperature has reached its minimum value, these backwarmed disks produce much more flux at 2.7 mm for a given size than the non-backwarmed models. We follow the same procedure described in § 2.2 to determine minimum sizes and masses and these are summarized in Table 1.

The required disk sizes are much smaller for the backwarmed viscous and reprocessing disks. To maintain consistency, envelope models were computed for the new sizes and new T_{eff} were computed. Here we encounter a problem of self-consistency; as noted by Keene and Masson, the *luminosity* added to the disk by backwarming is fictitious, since it will be reabsorbed by the envelope. If we included the new luminosity calculated from our "disk+star" model as a source for the envelope, we would no longer match the observed luminosity. Since a truly self-consistent calculation of the radiative transport for a disk inside an envelope is out of the question, we adopt the following expedient: we simply decrease the flux of the backwarmed disk at all wavelengths until the total luminosity of the star and disk matches the observed luminosity. This scaled spectrum is then fed into the radiative transport code as the central source when a new T_{eff} is computed for the envelope. We iterate the disk and envelope models until T_{eff} converges. The process converged rapidly to the values for R_{inner} and T_{eff} which are given in Table 2. We also present T_{inner}, the temperature for the inner edge of the envelope. Note that $T_{\mathrm{eff}} \sim 0.5 T_{\mathrm{inner}} \sim 100$ K for these envelopes, about two-thirds of the value assumed by Keene & Masson (1990).

The spectral energy distributions from the backwarmed disks are shown in Figure 3*a*. Note that the distinction between active disks and the others largely disappears, except at $\lambda < 50$ μm, where the emission is dominated by parts of the disk with $T > T_{\mathrm{eff}}$. The spectral energy distributions of the disks attenuated by the envelopes and the combined spectral energy distributions of the disk and envelope are shown in Figures 3*b* and 3*c*, respectively. Now all the disk models produce spectral energy distributions which are essentially identical, once placed inside the envelope, since the envelope properties are now nearly the same for all the disks (see Table 2).

The intensity distributions at various wavelengths were then compared to observations in the same way as for the models without backwarming. In general, the 50 and 100 μm scans are equally well matched by the backwarmed and non-backwarmed models. At 1.3 mm, the single beam data of Keene and Masson is matched slightly better by the backwarmed disks, particularly for the $T \propto r^{-0.5}$ disks. However, on the basis of data taken with large beams, one could not distinguish between backwarmed and nonbackwarmed models. The 1.3, 1.36, and 2.7 mm fluxes of all the backwarmed disk models are now identical. The 2.7 mm visibilities of the different disks with backwarming are now barely distinguish-

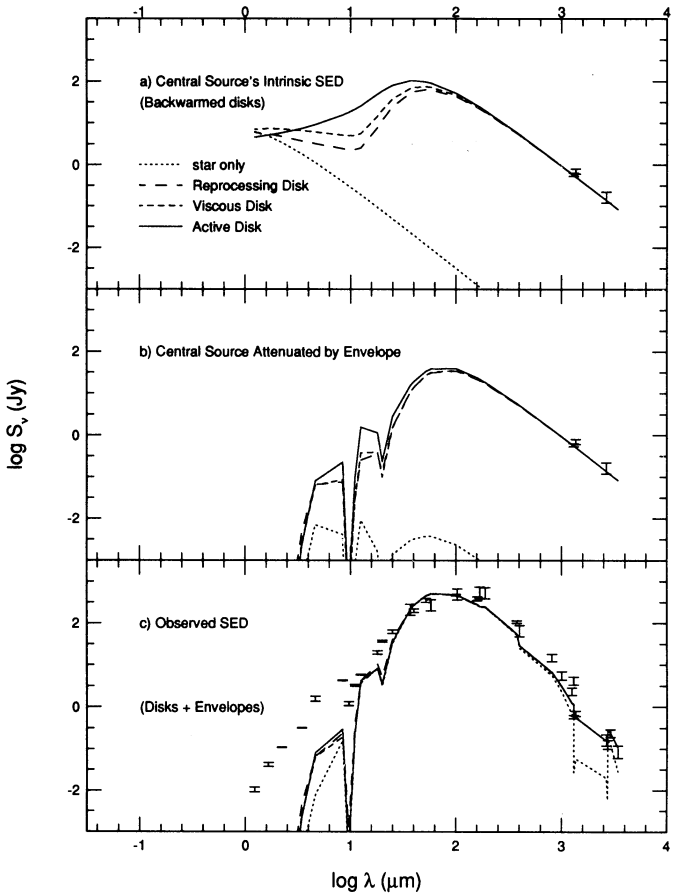

FIG. 3.—Same as Fig. 1, except that the disk temperature distributions have been calculated including backwarming by the envelope. Disk and envelope parameters are given in Tables 1 and 2.

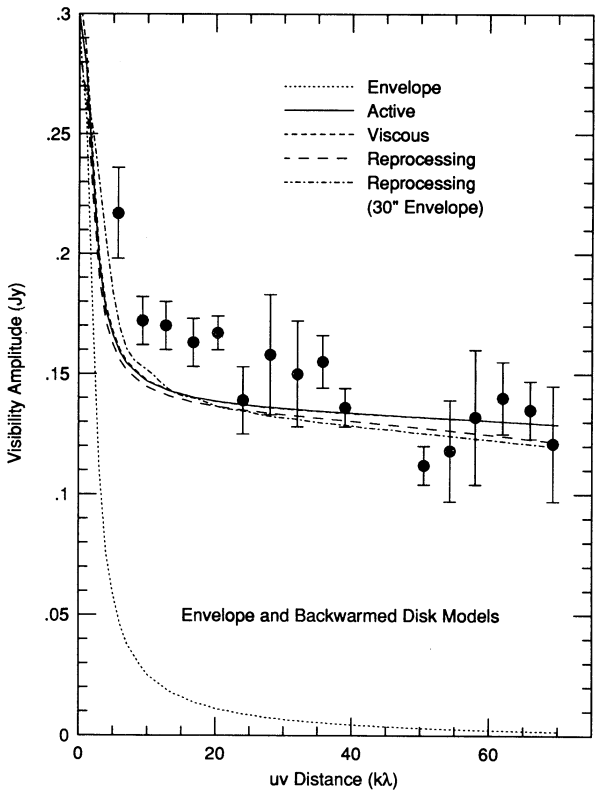

FIG. 4.—Same as Fig. 2, except that the disk temperature distributions have been calculated including backwarming by the envelope. The dot-dashed line is for a backwarmed, reprocessing disk inside an envelope with an outer radius of 30″.

able (see Fig. 4). The various backwarmed disk models have effectively produced the same long wavelength emission as the nonbackwarmed active disk model.

Backwarming by an envelope may have other consequences. For example, at a radius of 40 AU, the backwarmed viscous accretion disk has $T \sim 100$ K, whereas the nonbackwarmed viscous accretion disk has $T \sim 20$ K. Both the gas-phase chemistry and dust mantle chemistry would be very different at the higher temperature. Since comets in the solar system are thought to originate at distances of 40 AU, the different predicted disk temperatures will lead to very different thermal histories for comets. The temperature effects of backwarming on the inner regions of the disks (a few AU), however, are small. Natta (1993) discusses how an envelope can also alter the disk temperature profile through scattering radiation back onto the disk, and its importance for T Tauri systems. Backwarming and scattering provide natural mechanisms for a surrounding envelope to keep disks warm at large distances from the star.

Backwarming can also allow smaller disks to produce the observed emission, lowering the required disk masses, with consequences for other observational techniques. For example, Gómez et al. (1993) have failed to detect a compact source of NH_3 emission toward L1551 IRS 5. By assuming a disk size equal to their beam size ($\sim$64 AU) and an NH_3 abundance of 10^{-8}, they set an upper limit to the disk mass of 0.1 $M_\odot$. Since the backwarmed disks are all smaller than 64 AU, the resulting beam dilution will make their upper limit consistent with our lower limit, even with the nominal NH_3 abundance.

5. OTHER CONSIDERATIONS

5.1. *Effects of a Disk on the Derived Envelope Properties*

Butner et al. (1991) found that the best fit to the 100 μm scans was obtained for $\alpha = 1.5 \pm 0.3$ in models with only a star for the central source. The addition of a central source which produces significant amounts of emission at far-infrared and submillimeter wavelengths could affect this conclusion. To check this possibility, we have run models with values of α ranging from 0.5 to 2.0 for each central source model and compared them to the far-infrared scans and also the single-dish 1.3 mm map from Keene & Masson (1990). The best-fitting values of α lie in the range of 1.2 to 1.8. Considering all the data, we would assign a value of 1.4 ± 0.3 to α, in good agreement with Butner et al. (1991). This conclusion is the same regardless of which model is used for the central source.

We find that the conclusions reached by Butner et al. (1991) for the best value of α are unchanged by the addition of a disk, whether backwarmed or not. Essentially, the far-infrared emission in these scans and maps is dominated by the envelope and the nature of the central source is unimportant even for the largest sources (the reprocessing disk) and the sources with the most intrinsic emission at 100 μm (the blackbody and the active disk). Only when one has high-resolution data, such as provided by millimeter interferometer data, can one pick out the disk emission as a separate, necessary component. We con-

clude that studies of the spatial distribution of the envelope in the far-infrared with resolutions of 10″ to 20″ are not sensitive to the presence or nature of a disk.

One possible impact on envelope properties is suggested by the failure of any of our models to match the visibilities at baselines ranging from 7–25 $k\lambda$. Since these baselines were better matched by the simple model of Keene & Masson (1990), consisting of a Gaussian core inside a power law envelope cut off at 30″, we have tried a model where the envelope has an outer radius of 30″. The visibilities of this model, which uses a backwarmed reprocessing disk, come closer to the observations in the range of 7–25 kλ, but do not match them (see Fig. 4). The simple model of Keene and Masson apparently achieved its success in this region mostly by allowing the central Gaussian and the power-law envelope to both contribute in this region, since they intermingled; the physical meaning of such a model is questionable.

Is there any basis for cutting off the envelope at 30″? The molecular cloud is clearly much more extensive. One rationale for a change, if not a cutoff, on that scale is theoretical: the radius marking the boundary of the infall zone for the ALS model of L1551 is 21″; at this point, the density power law should steepen to $n(r) \propto r^{-2}$. We modified our density distribution and recalculated the emission expected at millimeter wavelengths, but the broken-power law does not improve the fit to the uv visibilities. An alternate possibility is suggested in Figure 2, where a large disk (199 AU radius) fits the 7–25 kλ visibilities, though it does not match well at larger uv visibilities. Thus, if there were some additional emission over what our various disk models would predict on size scales of 200–300 AU, we could match the millimeter visibilities. The continuum emission might be associated with the inner regions of the $C^{18}O$ emission seen by Sargent et al. (1988). The $C^{18}O$ emission has a radius of about 700 AU and has a flattened structure. The region may represent the portion of the collapsing envelope where the departures from spherical symmetry become noticeable.

5.2. *Effects of Different Dust Opacities*

We have seen above that adding a compact source to models of the envelope emission can substantially improve the fit to the long wavelength data, but that the fit to the mid-infrared observations is still poor. In contrast, Butner et al. (1991) showed that different assumptions about the dust opacities could have a large effect in the mid-infrared, but the implications were not fully explored. In particular, the dust opacities of Mathis et al. (1983) provided a better match to the mid-infrared observations in the pure envelope models, but it was not clear how the combination of these opacities with a disk would fare. Since we now have the capability to consider these together, we return to the issue of dust opacities.

So far in this paper, we have used the modified dust opacities of Adams et al. (1987) (hereafter "ALS dust"); examination of Figure 12 of Butner et al. (1991) shows that the far-infrared (100 μm) opacities of ALS dust are intermediate between those advocated by Mathis et al. (1983) (hereafter "MMP dust") and the commonly used opacities of Draine & Lee (1984) (hereafter "DL dust"). The key difference is in the ratio of far-infrared opacity to the opacity at shorter wavelengths. The opacities of MMP dust have the highest value of this ratio, and DL opacities have the lowest value. Since the far-infrared emission constrains the optical depth at 100 μm, the MMP dust will have much less opacity than DL dust at mid-infrared wavelengths. While DL dust has too much optical depth, and MMP too little optical depth when compared to the current average interstellar dust opacity law (Mathis 1990), we have found that both DL and MMP dust models are consistent with far-infrared data, within the observational uncertainties. To explore the effects of these differences, we have run a series of models with different α for each dust model and for each model of a central source. We remind the reader that the ALS dust opacities were modified to reproduce the observations in large beams by changing the dust opacity law to go as ν^1 at wavelengths longer than 700 μm. To inhibit our peregrinations through parameter space, we will adopt the same long-wavelength modification for both DL and MMP dust opacity models.

First we consider the effects of different dust opacities on the conclusions Butner et al. (1991) reached about the value of α which best fits the big beam far-infrared and 1.3 mm (Keene & Masson 1990) intensity distributions. For DL dust, the conclusions are unchanged from those based on ALS dust; the best value is $\alpha = 1.4 \pm 0.3$. The ALS and DL 100 μm optical depths for the models are similar, due to the fact that the ALS and DL far-infrared opacities are almost identical. In contrast, MMP dust requires slightly higher 100 μm optical depths. In the case of MMP dust, the far-infrared data are fitted better by a lower $\alpha \sim 1$–1.2, while the 1.3 mm big beam data are still well-fitted by $\alpha \sim 1.5$. Overall, a smaller value of α is favored (1.2 ± 0.3). The tendency of MMP dust to favor smaller values of α was also found in our study of NGC 2071 (Butner et al. 1990). It occurs because the temperature distribution is somewhat different (see Fig. 3 of Butner et al. 1990); in particular, the temperatures at large radii are lower for MMP dust than for DL dust, requiring a slower decrease in the density (and by extension the optical depth) to match the observations. These conclusions about the best value of α are independent of the choice of central souce.

What effects do these different opacity laws have on the spectral energy distribution? Figure 5 shows the spectral energy distribution computed with the best-fitting model for both of the alternative dust models, with the same model of a backwarmed active disk for the central source. Only in the case of the MMP dust is the disk radiation seen through the envelope. DL-type dust has too high an opacity to see the mid-infrared emission through the envelope, contrary to the arguments of ALS. The combination of the active disk and the dust opacities of MMP clearly provides the best match to the data from 3 μm to 3 mm. However, since an envelope alone can produce enough mid-infrared emission (Butner et al. 1991), the mere presence of the mid-infrared is not a guarantee of the existence of a disk in a deeply embedded source like L1551 IRS 5. The agreement at wavelengths between 200 and 1000 μm is noticeably better for the dust of Mathis et al. (1983) because the smaller value of α provides somewhat more emission in that range of wavelengths. The modified Draine & Lee (1984) dust opacities, on the other hand, fit the data much more poorly in the mid-infrared, given the same underlying disk model. If we look for the best possible DL model among the cases we consider, the nonbackwarmed, viscous disk model does best at matching the observed spectral energy distribution. This model produces the most mid-infrared flux because the envelope is relatively thin (unlike the backwarmed cases or the nonbackwarmed active disk) and the disk is warmer than the reprocessing case. However, even this DL-dust model *fails* to reproduce the observed mid-infrared flux, and this model also cannot match the visibilities at 2.7 mm as well as more compact disk models do.

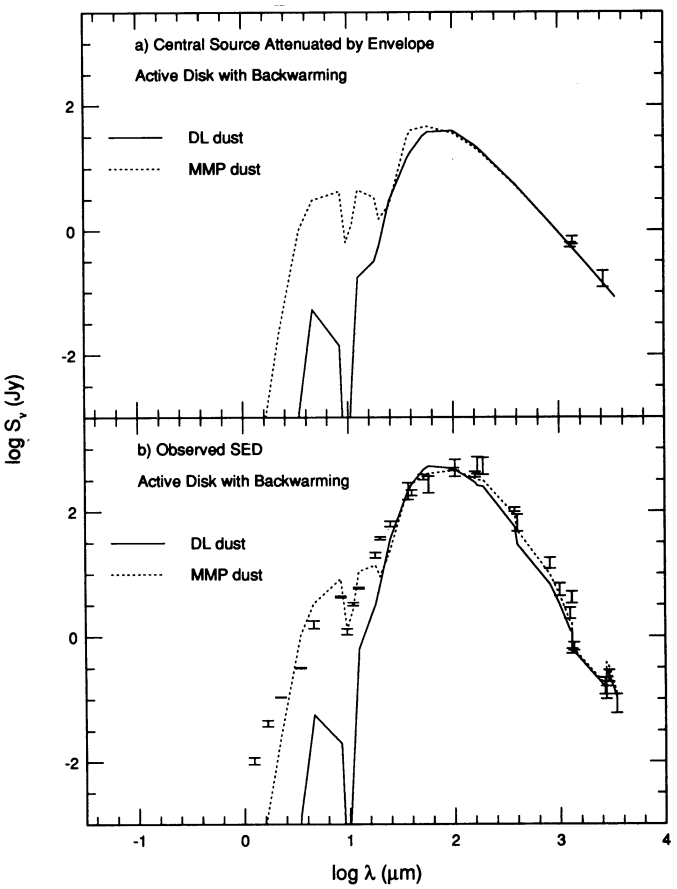

FIG. 5.—(*a*) Predicted spectral energy distributions of the disks attenuated by the envelope are presented for two models of the dust opacities, those of Mathis et al. (1983) (*dotted line*) and those of Draine & Lee (1984) (*solid line*). In both cases, the central source is the backwarmed, active disk of Fig. 3(*a*). (*b*) The total observed spectral energy distributions (including the envelope emission) are presented for the two dust opacity models: Mathis et al. (1983) (*dotted line*) and Draine & Lee (1984) (*solid line*).

Can we conclude from these results that the mid-infrared to far-infrared ratio of dust opacities proposed by Mathis et al. (1983) is "correct"? This conclusion would be too facile, since we have fit the data of only one source with an admittedly simplified source model. For example, it could be possible for the dust opacities of Draine & Lee (1984) to provide a better fit if some of the mid-infrared radiation arises in shock-heated material in the outflow. In addition, departures from spherical symmetry could help the DL dust model to fit better, by allowing more mid-infrared light to scatter out the poles of the outflow, although scattering in the mid-infrared should be very weak for DL grains.

6. SUMMARY

We have constructed three types of disk models (reprocessing, viscous accretion, and "active") and considered the observational effects of placing them inside a spherical envelope. In particular, we have applied this technique to model the emission from L1551 IRS 5. We modified the ALS, MMP, and DL dust laws to fit big beam observations at 2.7 mm while simultaneously using the disk emission to reproduce the observed 2.7 mm interferometer flux. We find that the effects of the disk on previous conclusions about the density distribution in the envelope, derived from big beam far-infrared observations, are minimal. On the other hand, the envelope of a heavily embedded source like L1551 IRS 5 can have a major effect on derived disk properties. Except for the case of MMP dust opacities, the envelope is able to obscure the disk completely, either by attenuation or by overwhelming its radiation, at all wavelengths except those longer than about 1 mm. Even at 2.7 mm, the disk is seen clearly only with interferometric observations. In addition, the envelope can have a substantial backwarming effect on the disk, thereby tending to produce a flatter temperature distribution at the outer edges of the disk. The differences between various disks then become irrelevant since the millimeter flux is dominated by the outer, backwarmed disk. As a result, backwarmed disks, if more generally relevant, may prevent current observations from distinguishing between different physical models for the internal disk luminosity for deeply embedded young stellar objects. In addition, if backwarming is generally important, the thermal history of the outer disks of planetary systems may be affected.

We would like to thank Colin Masson, Pat Cassen, and Lynne Deutsch for helpful discussions. We would like to thank Anneila Sargent for providing us with her 1.3 mm interferometer data in advance of publication. We are especially grateful to Shudong Zhou for writing the code which calculated visibilities from model intensities. This work was supported by NASA grants NAG2-420, NAGW-2323, and ASI grant ASI-90-RS-46. Harold M. Butner was supported by a National Research Council Fellowship.

REFERENCES

Adams, F. C., Lada, C. J., & Shu, F. H. 1987, ApJ, 312, 788
———. 1988, ApJ, 326, 865
Adams, F. C., Ruden, S. P., & Shu, F. H. 1989, ApJ, 347, 959
Beckwith, S. V. W., Sargent, A. I., Chini, R. S., & Gusten, R. 1990, AJ, 99, 924
Butner, H. M., Evans, N. J., II, Harvey, P. M., Mundy, L. G., Natta, A., & Randich, M. S. 1990, ApJ, 364, 164
Butner, H. M., Evans, N. J., II, Lester, D. F., Levreault, R. M., & Strom, S. E. 1991, ApJ, 376, 636
Calvet, N., Magris, C. G., Patiño, A., & D'Alessio, P. 1992, Rev. Mexicana Astron. Af., 24, 27
Draine, B. T., & Lee, H. M. 1984, ApJ, 285, 89
Egan, M. P., Leung, C. M., & Spagna, G. F., Jr. 1988, Comput. Physics Comm., 48, 271
Gómez, J. F., Torrelles, J. M., Ho, P. T. P., Rodríguez, L. F., & Cantó, J. 1993, ApJ, 414, 333
Hartmann, L., Kenyon, S. J., & Calvet, N. 1993, ApJ, 407, 219
Hillenbrand, L. A., Strom, S. E., Keene, J., & Vrba, F. J. 1992, ApJ, 397, 613
Keene, J., & Masson, C. R. 1990, ApJ, 355, 635
Kenyon, S. J., & Hartmann, L. 1987, ApJ, 323, 714
———. 1991, ApJ, 383, 664
Ladd, E. F., Adams, F. C., Casey, S., Davidson, J. A., Fuller, G. A., Harper, D. A., Myers, P. C., & Padman, R. 1991, ApJ, 366, 203
Mathis, J. S. 1990, ARA&A, 28, 37
Mathis, J. S., Mezger, P. G., & Panagia, N. 1983, A&A, 128, 212 (MMP)
Moneti, A., Forrest, W. J., Pipher, J. L., & Woodward, C. E. 1988, ApJ, 327, 870
Natta, A. 1993, ApJ, 412, 761
Natta, A., Palla, F., Butner, H. M., Evans, N. J., II, & Harvey, P. M. 1992, ApJ, 391, 805
———. 1993, ApJ, 406, 674
Pollack, J. B., Hollenbach, D., Simonelli, D., Beckwith, S., Roush, T., & Fong, W. 1994, ApJ, submitted
Sargent, A. I. 1991, private communication
Sargent, A. I., Beckwith, S., Keene, J., & Masson, C. 1988, ApJ, 333, 936
Shu, F. H. 1977, ApJ, 214, 488
Shu, F. H., Adams, F. C., & Lizano, S. 1987, ARA&A, 25, 23
Snell, R. L. 1981, ApJS, 45, 121
Stocke, J., Hartigan, P. M., Strom, S. E., & Strom, K. M. 1988, ApJS, 68, 229
Terebey, S., Shu, F. H., & Cassen, P. 1984, ApJ, 286, 529
Woody, D. P., Scott, S., Scoville, N. Z., Mundy, L. G., Sargent, A. I., Padin, S., Tinney, C. G., & Wilson, C. D. 1989, ApJ, 337, L41